JOURNAL OF GEOPHYSICAL RESEARCH, VOL. 98, NO. C2, PAGES 2393–2406, FEBRUARY 15, 1993

# Long-Period Transport Changes in the Eastern North Atlantic and Their Simulation by Propagating Waves

GEROLD SIEDLER AND MICHAEL FINKE

*Institut für Meereskunde, Kiel, Germany*

An analysis is presented of geostrophic volume transport across a zonal line along 28°N in the eastern Atlantic. The data are from an array of five moorings with 200-km spacing carrying temperature sensors and one current meter each for 1 or 2 years. Transport changes in the main thermocline relative to a fixed depth level are obtained by the use of temperature-salinity relationships. The transport variability is simulated by two propagating waves with first-order baroclinic mode structure. Solutions exist with annual and semi-annual periods and zonal wavelengths of 100–200 km and 300 km, respectively. Assuming quasi-geostrophic dynamics and using results on the Reynolds stress, the dominating waves of annual and semi-annual period are found to propagate to the southwest, with 45°–60° and 25° to the south off the westward direction, respectively. Wave solutions with a 90-day period and a zonal wavelength of about 300 km are interpreted as an effect of barotropic waves arising due to horizontal temperature inhomogeneity. The propagation is about ±25° off the westward direction. In general, good approximations are obtained with the propagating wave simulations in the western and central part of the array, while large differences occur between observation and simulation close to the Canary archipelago. Possible causes for these differences are discussed.

## 1. INTRODUCTION

Ocean current spectra from long-term moorings usually exhibit high energies at three different ranges of scales: in the range between a few days and about 1 hour the high energy will be due to internal gravity, tidal, and inertial waves; in the range of about 50–100 days, energy is attributed primarily to mesoscale eddies, planetary waves, and equatorial waves in the tropics; and at longer periods, Rossby waves are considered the main cause. In Figure 1 we reproduce spectra in energy-preserving form obtained by *Müller and Siedler* [1992] from almost 9 years of current meter records at mooring KIEL276 in the eastern North Atlantic, close to the area of the present study [see also *Schmitz et al.*, 1988]. The position of the mooring is displayed in the map in Figure 2. The spectra represent the barotropic and first-order baroclinic dynamical modes at frequencies below inertial. Maxima of energy are apparent in the range between approximately 50 days and about 1 year. The two modes account for about 90% of the total velocity variance at low frequencies on this position. The first three modes of horizontal velocity are also reproduced from *Müller and Siedler* [1992] in Figure 3. In the main thermocline the velocity of the first-order baroclinic mode is larger than the barotropic and the second-order baroclinic velocity. The mean velocity in this region in the upper ocean is of order 1 cm/s [*Stramma*, 1984]. The first-order baroclinic component will thus provide at least about half of the low-frequency current contributions. It can be determined from the density gradients and the related geostrophic currents at selected main thermocline levels by fitting these data to first-order dynamical modes. It has been shown by *Emery and Dewar* [1982] and *Siedler and Stramma* [1983] that stable temperature-salinity ($T$-$S$) relationships exist in this region in the North Atlantic Central Water (or in the main thermocline). Density and geopotential anomaly fields in the upper ocean can therefore be well approximated here from temperature data by applying the known $T$-$S$ relationships.

The present study uses temperature time series from a zonal array of moored thermistor cables at 28°N to the west of the Canary Islands. It is our aim to determine contributions to the flow in the low-frequency range. Wave contributions will probably dominate at these long periods. The wave properties obtained from fitting observational data will be compared to Rossby wave dynamics. Our data set does not permit us to determine the relevant generation processes, but we will briefly review the possible generation mechanisms that have been proposed earlier.

A description of the internal oceanic wave field can be obtained by formulating a model with a superposition of propagating waves, and then fitting the data to the model by selecting the appropriate free parameters of the model. The fitting can be performed in the frequency domain [e.g., *Emery and Magaard*, 1976] or in the time domain [e.g., *McWilliams and Flierl*, 1976]. *Price and Magaard* [1983] discussed both alternatives. In their analysis of a Pacific Ocean expendable bathythermograph (XBT) data set from the area between Honolulu and San Francisco, they compared the stochastic approach using simulated Rossby waves with the deterministic approach of *White and Saur* [1981]. The results from both methods were basically consistent. The deterministic approach, however, provided a better approximation near the continental slope off the coast of the United States, i.e., close to the probable source region of westward propagating baroclinic Rossby waves. Our 28°N moorings are in a similar situation near the corresponding source region off the African coast in the Atlantic Ocean. Considering the scales of variations and the limited length of our records, only the second (deterministic) approach is feasible in this study.

Empirical results on Rossby waves have mostly been



Paper number 92JC02122.
0148-0227/93/92JC-02122$05.00

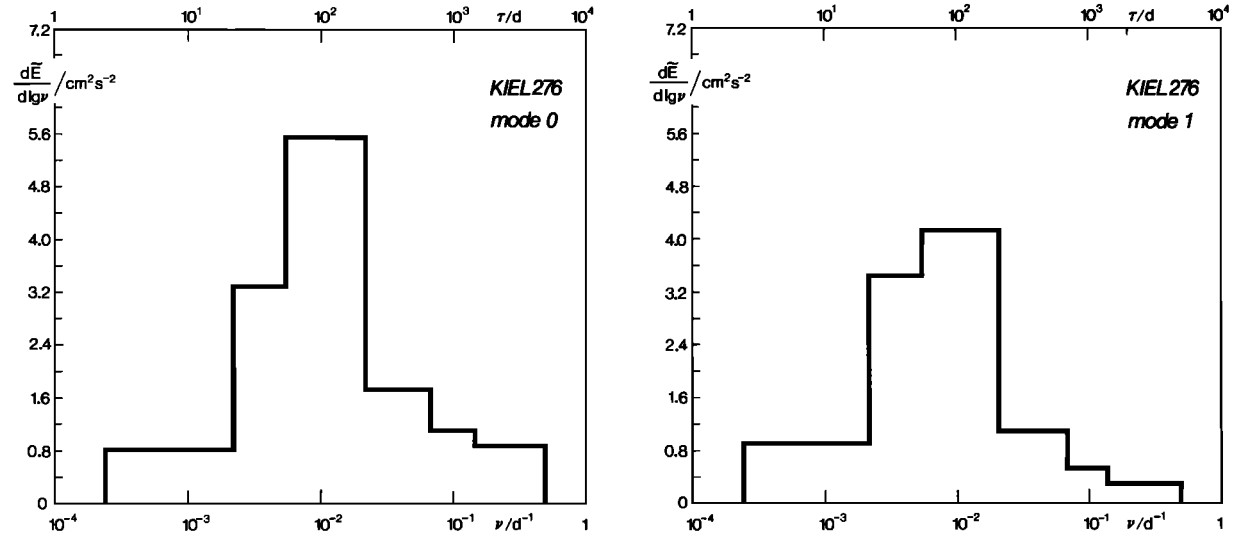


Fig. 1. Energy-preserving spectra of the barotropic and first baroclinic modes at mooring KIEL276 in the northern Canary Basin [after *Müller and Siedler*, 1992], with $\bar{E}$ the energy, $\nu$ the frequency, and $\tau$ the period.

obtained for the Pacific. We refer to the following analyses: *Emery and Magaard* [1976], *Magaard and Price* [1977], *Magaard* [1977, 1983], *White* [1977, 1982], *Kang and Magaard* [1979, 1980], *White and Saur* [1981], and *Price and Magaard* [1983]. Using large-scale temperature data sets, evidence was found in these studies for considerable first-order baroclinic contributions of waves with annual periods and wavelengths of approximately 1000 km, but with some contributions also of wavelengths of about 300 km. There were also indications of semiannual and longer than annual wave components. Observations from the Mid-Ocean Dynamics Experiment (MODE) and the polygon MODE (POLYMODE) have been used to study Rossby waves in the North Atlantic [*MODE Group*, 1978]. *McWilliams and Robinson* [1974] described the structure of eddies which could be well simulated by a superposition of two first-order baroclinic Rossby waves. *McWilliams and Flierl* [1976] used one barotropic and two first-order baroclinic waves for a simulation of a moored data set and were able to approximate up to 90% of the observed fluctuations.

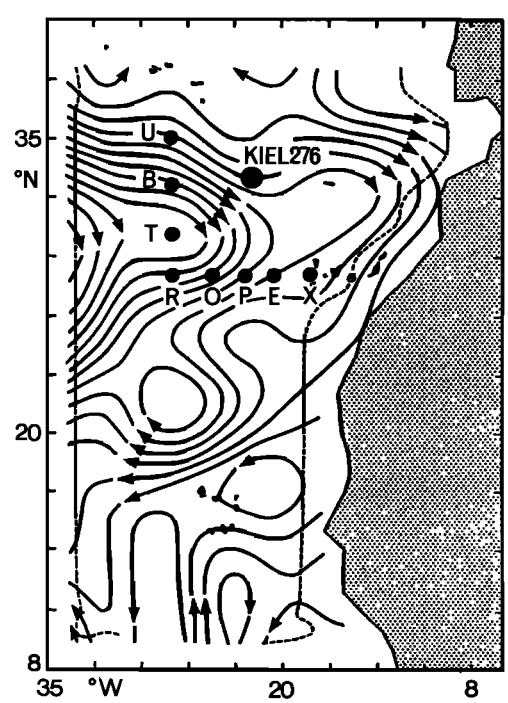


Fig. 2. Map of observational area, with locations of moorings U, B, T, R, O, P, E, X, and KIEL276 and mean 0- to 800-m geostrophic volume transports from hydrographic data [after *Stramma*, 1984]. Transport between lines is $10^6$ m$^3$ s$^{-1}$.

## 2. Experiment Design

In order to determine mass transport changes in the main thermocline using the *T-S* method, an array of vertical temperature cables was moored in the northern Canary Basin. The positions of the moorings U, B, T, R, O, P, E, X are given in Figure 2 and Table 1. They were selected with the intention of crossing the mean gyre flow, with a meridi-

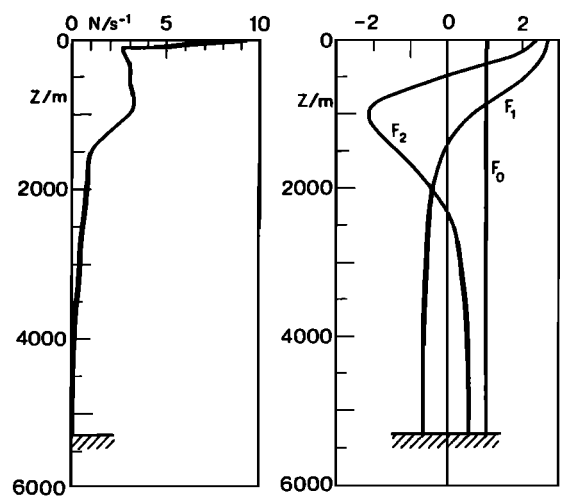


Fig. 3. Mean vertical Brunt-Väisälä frequency ($N$) profile and dynamical modes $F_0$, $F_1$, and $F_2$ at mooring KIEL276 [after *Müller and Siedler*, 1992].

TABLE 1. Mooring and Approximate Hydrographic Station Position, Mooring Observational Period, Nominal Instrument Depth of Uppermost Temperature Sensor, Instrument Performance, and Common Periods

| Mooring | Latitude, deg N | λ, °W | Phase | Period | | Depth, m | Comment |
|---|---|---|---|---|---|---|---|
| | | | | Start | End | | |
| U | 35°01.8′ | 26°28.9′ | 2 | Nov. 4, 1984 | Sept. 28, 1985 | 170 | |
| B | 32°38.9′ | 26°30.5′ | 2 | Nov. 2, 1984 | May 4, 1985 | 180 | Current and temperature record short |
| T | 30°21.3′ | 26°29.2′ | 2 | Nov. 1, 1984 | Sept. 28, 1985 | 230 | |
| R | 28°00.4′ | 26°29.1′ | 1 | Oct. 27, 1983 | Oct. 28, 1984 | 350 | |
| | | | 2 | Nov. 5, 1984 | May 12, 1985 | 210 | Temperature record short |
| O | 28°00.3′ | 24°30.0′ | 1 | Oct. 26, 1983 | Oct. 30, 1984 | 285 | |
| | | | 2 | Nov. 7, 1984 | Sept. 28, 1985 | 300 | |
| P | 27°59.3′ | 22°23.4′ | 1 | Oct. 25, 1983 | Oct. 31, 1984 | 270 | Current record short |
| | | | 2 | Nov. 8, 1984 | Sept. 28, 1985 | 230 | |
| E | 28°00.8′ | 20°25.5′ | 1 | Oct. 29, 1983 | Nov. 1, 1984 | 320 | |
| | | | 2 | Nov. 9, 1984 | Aug. 17, 1985 | 260 | |
| X | 28°00.9′ | 18°18.3′ | 2 | Nov. 10, 1984 | Sept. 27, 1985 | 190 | Current record short |

Depth ranges and periods selected for the analysis are TK1, Oct. 30, 1983, to Oct. 28, 1984, at 350–710 m; and TK2, Nov. 10, 1984, to Sept. 25, 1985, at 260–620 m.

onal line of moorings at 26.5°W (U, B, T, R) and a zonal line at 28°N (R, O, P, E, X). A schematic presentation after *Klein and Siedler* [1989] of the large-scale flow in this extension of the Gulf Stream system is given in Figure 4. Our observational area is located at the lower right corners of these maps.

A typical mooring is shown in Figure 5. Thermistor cables, each 400 m long and with 10 equidistant temperature sensors, were attached to the mooring line at approximately 200- to 600-m depth in the main thermocline. The recorder on top of the cable also carried a pressure sensor. This allowed the determination of depth variations due to changing mooring-line inclination which is caused by varying current drag. One current meter each was placed above the thermistor cable recorder. A second thermistor cable was attached at greater depth, usually 800–1200 m, for a study of the Mediterranean Water component in the North Atlantic Deep Water. Aanderaa instruments were used in all moorings. Measurements covered the time period from October 1983 to October 1984 (phase 1) and from November 1984 to July 1985 (phase 2), with 1-year observations at the meridional and nearly 2 years of observations at the zonal line.

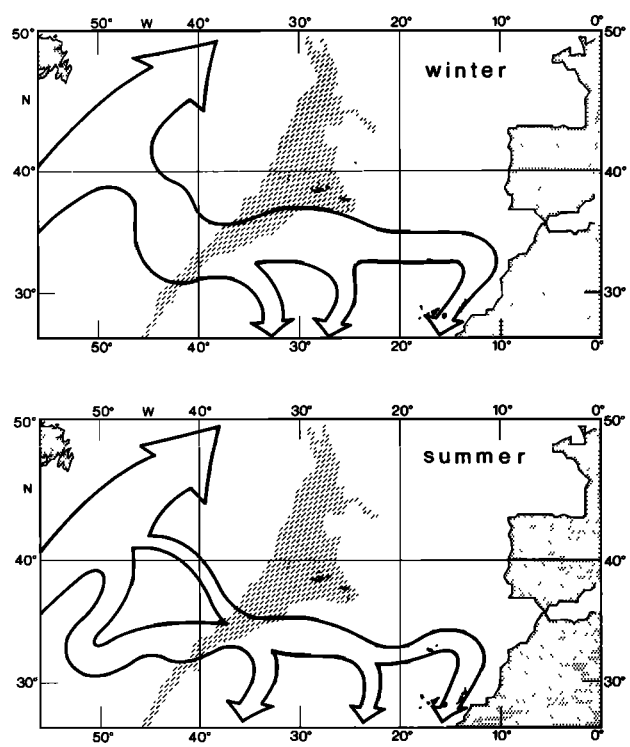


Fig. 4. Schematic presentation of the flow in the upper ocean on a larger scale [after *Klein and Siedler*, 1989].

Only data from the main thermocline levels will be used in the present study. Details of mooring position, measurement period, nominal instrument depth, and instrument performance are presented in Table 1 and Figures 6 and 7. In addition to the moored instrument time series, CTD profiles were obtained at selected positions, particularly near the moorings at the times of launching and retrieval, and also earlier in 1983. The stations are summarized in Table 1 and Figure 2.

## 3. Data Processing

Temperature and pressure of the moored instruments were sampled at 2-hour intervals. Data were quality controlled, and obviously erroneous values were rejected. The time series were then low-pass filtered with a cutoff period of approximately 2 days in order to eliminate short-periodic variability, particularly internal gravity waves with tidal periods.

The actual depth of the individual measurement had to be determined from the pressure records because of sensor depth changes of up to 30 m during the observational period. A correction scheme was applied, assuming a rigid pendulum approximation (see Figure 8). The vertical displacement $\Delta z_i$ of a sensor ($i$) below the respective pressure sensor ($l$) will be smaller than $\Delta z_l$ by a factor $l_i/l_l$, with $l_i$ and $l_l$ being the respective bottom distances of the sensors in the case of a vertical mooring line. The corrected temperature $T_i$ at a minimum depth $z_i$ for sensor $i$ at time $t$ is then obtained from the temperature $T_{mi}$ measured at depth $z_{mi}$:

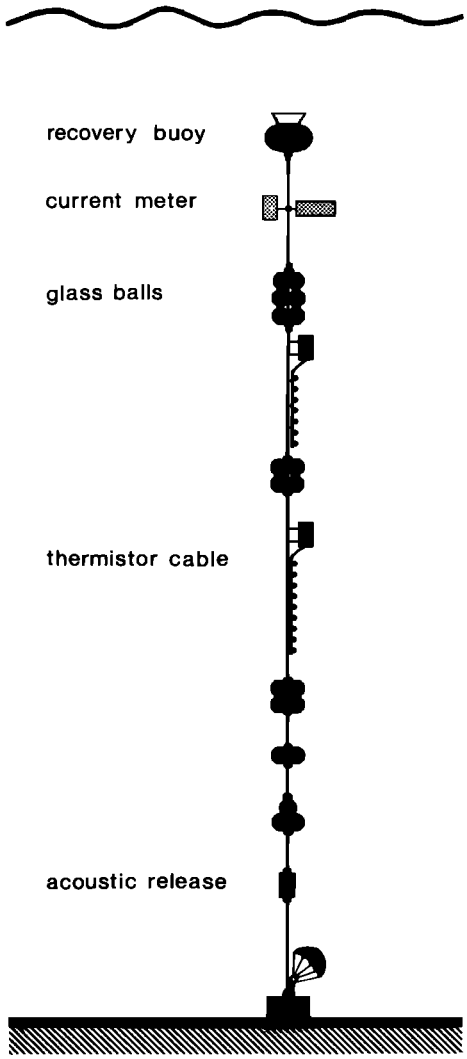


Fig. 5. Typical thermistor cable mooring.

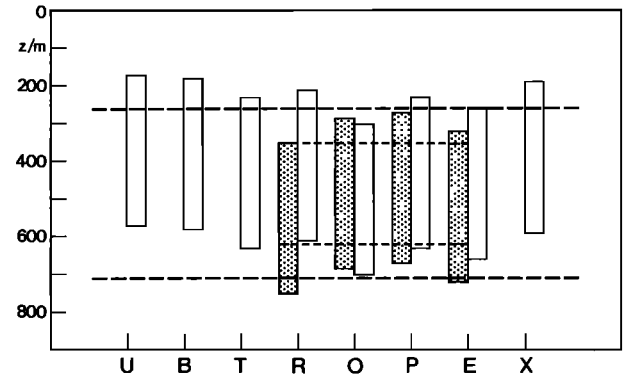


Fig. 7. Vertical coverage by thermistor cables at moorings U–X during phase I (dotted columns) and phase II (open columns). The horizontal lines indicate depth ranges used in the analysis.

$$T_i(z_i, t) = T_{mi}[z_{mi}(t), t] + \frac{\overline{\partial T(t)}}{\partial z}\Delta z_i(t) \qquad \Delta z_i = \frac{l_i}{l_l}\Delta z_l \tag{1}$$

The vertical gradient $\partial T/\partial z$ was determined from the corresponding thermistor cable data set, averaging over 24 hours. The corrected temperatures were then linearly interpolated for each time step in order to obtain temperatures at levels common for all moorings used in the analysis: 350–710 m in phase 1 and 260–620 m in phase 2 (see Figure 7). In some cases extrapolation by as much as two depth increments (2 × 40 m) was necessary, but was considered uncritical because of the almost linear vertical temperature variation in the respective depth range. Comparisons of the depth-corrected time series with conductivity, temperature, and depth (CTD) data at specific times indicated deviations which are typically as small as 0.05°C.

## 4. Volume Transports

In earlier studies of mean geostrophic transports by *Stramma* [1984] and *Klein and Siedler* [1989] it was shown that a level of no motion at 1300–1500 m leads to good approximations of the transport field in the upper ocean in this region. Stramma found a difference in mean transports of less than 12% when replacing the above reference level by

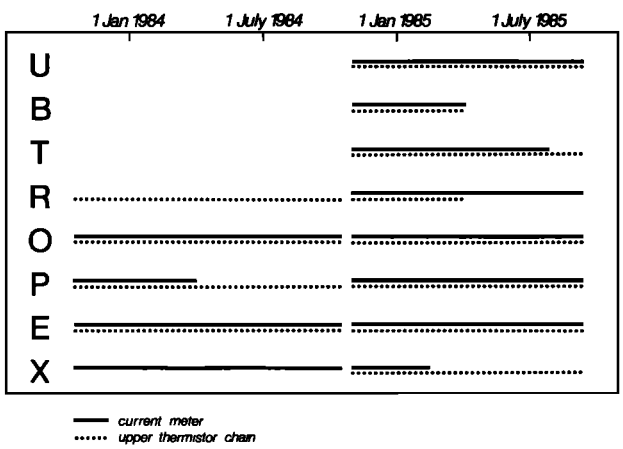


Fig. 6. Summary of current meter and thermistor cable data in the array. For locations see Figure 2.

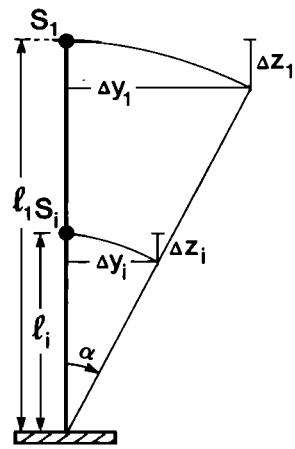


Fig. 8. Definition of terms for the correction of sensor depth changes.

TABLE 2. Hydrographic Stations

| Vessel | Cruise | Year | Data |
|---|---|---|---|
| *Meteor* | 64 | 1983 | CTD's along 28°N |
| *Poseidon* | 104 | 1983 | CTD's along 28°N |
| *Meteor* | 69 | 1984 | CTD's, XBT's in whole area |
| *Polarstern* | 5 | 1985 | CTD's along 28°N |

2000 m. A change of reference levels by several hundred meters will thus only introduce small deviations. In order to obtain a first view of transport changes, we will assume that such a selection is also appropriate for the low-frequency variability of transports. This will also provide the opportunity to check whether the mean of consecutive CTD surveys results in transport numbers comparable to the above studies.

Geostrophic transports were calculated relative to 1500 m for the four CTD data sets which are summarized in Table 2. The results are presented in Figure 9. The four individual CTD surveys lead to the transport rates shown in Figures 9*a*–9*d*. The transports are highly variable zonally and from one survey to the next. The temporal mean in Figure 9*e* indicates a maximum southward transport between moorings O and P and a northward transport near the Canary Islands between moorings E and X, opposite to the mean flow obtained in *Stramma*'s [1984] maps. It should be noted that Stramma used 3° × 3° squares for averaging and an objective analysis scheme with a correlation scale of 470 km. His fields will therefore not resolve the flow in our array. The cumulative transport, starting integration from the westernmost point, is presented in Figure 9*f*. It is directed southward, adding up to 2.5 Sv (1 Sv = $10^6$ $m^3/s$). This number is reasonably close to the 3 Sv transport in the layer 0–800 m (with deeper reference level) that can be deduced from *Stramma*'s [1984] analysis (see Figure 2). We conclude that transports are characterized by a mean southward flow with variations exceeding the mean, and that the eastern part of the section is probably governed by different dynamics, compared to the central and western part.

We will next determine geostrophic transports from the thermistor cable time series using mean *T-S* relationships. Individual *T-S* distributions of the CTD profiles are presented in Figure 10 for 26.5°W and 28°N. The hatched areas

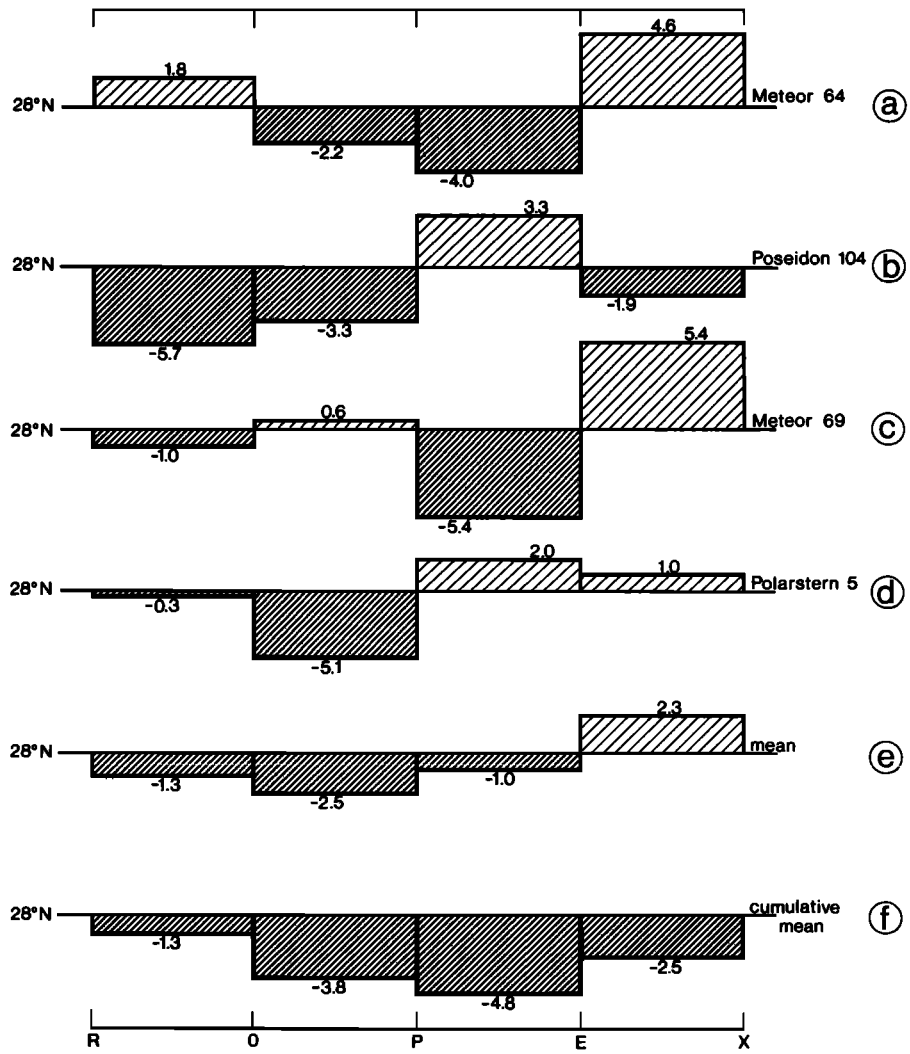


Fig. 9. (*a–d*) Volume transports between sites R, O, P, E, X (see Figure 2) perpendicular to latitude 28°N from four CTD surveys, (*e*) temporal mean transports, and (*f*) cumulative transport.

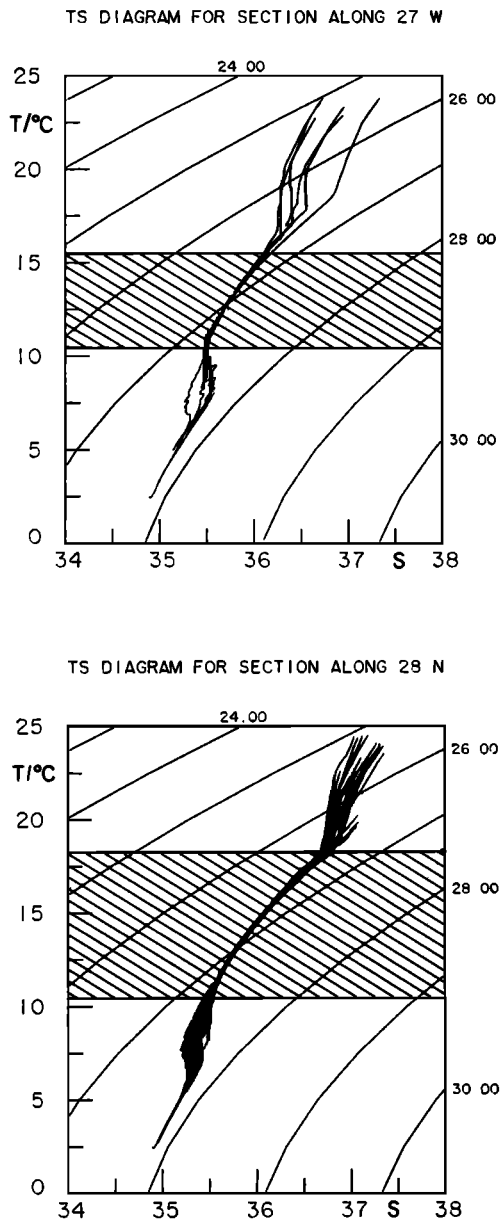


Fig. 10. Temperature-salinity ($T$-$S$) distributions from CTD's on mooring sites (top) along 26.5°W and (bottom) along 28°N. The hatched areas indicate ranges of temperature time series used in this study.

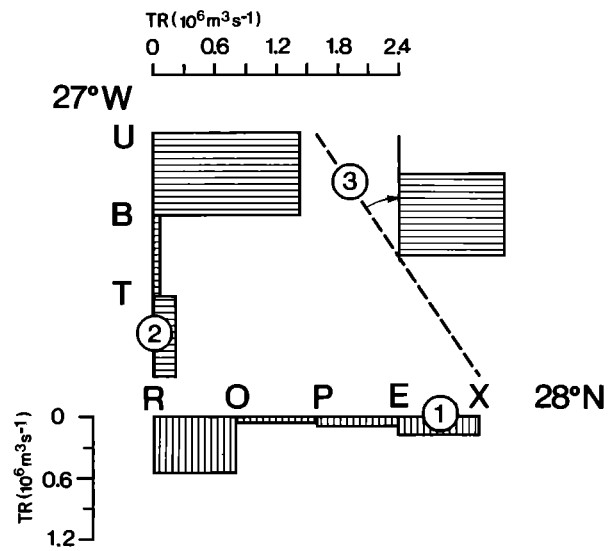


Fig. 11. Volume transports (TR) between 260- and 620-m depth determined from geostrophic currents relative to a 620-m reference level for the observational period 1984–1985: 1, across 28°N; 2, across 27°W; and 3, across line between moorings U and X.

indicate the temperature ranges in the thermistor cable data. It is obvious from these graphs that temperature can be well related to density in these ranges. For a detailed discussion of errors, we refer to *Siedler and Stramma* [1983]. In the following study of transport variability we will avoid extrapolation to the 1300- to 1500-m reference levels used for mean transport calculations, and will examine "relative transports," i.e., volume transports which are calculated from geostrophic currents in a 360-m-thick layer relative to the lower boundary of this layer. The mean relative transports for this layer are summarized in Figure 11. The error analysis leads to an rms error of ±0.2 Sv. These relative transports will be lower than the absolute transports.

In addition to the values for adjacent mooring pairs, the transport to the northeast across the line U-X is also included. Qualitatively, we find an inflow into the triangle U-R-X in the northern part from the west, corresponding to the Azores Current [*Käse and Siedler*, 1982; *Käse et al.*, 1985; *Gould*, 1985], and a partition into an outflow to the northeast and an outflow to the south of approximately equal magnitude. These two outflows correspond to two branches of the Azores Current [*Klein and Siedler*, 1989]. We conclude that the mean relative transports from this analysis are consistent with earlier results on the mean geostrophic flow in the main thermocline in this region, both with respect to spatial pattern and approximate magnitude.

Relative transport time series for the main thermocline layers are presented in Figures 12 and 13. One recognizes strong variations on time scales from a few months to 1 year. They can be caused by long-periodic waves or, particularly on the shorter time scales, by mesoscale eddies. We will attempt to simulate the observed transport variations by propagating long-periodic waves. Because of the longer time series and the better spatial coverage on the line along 28°N compared to the line along 26.5°W, we will only use the zonal section data for the following wave analysis.

## 5. Wave Model

Considering the results described earlier in the introduction, an approximation of baroclinic volume transport variations by a superposition of first-order propagating waves appears both appropriate and feasible in our case. We will first check the scales to be expected. The dispersion relation for baroclinic Rossby waves of first-order mode [e.g., *Leblond and Mysak*, 1978] is given by

$$\omega = -\frac{\beta\kappa}{k^{*2} + R^{-2}} \qquad R = \frac{NH}{f\pi} \tag{2}$$

with angular frequency $\omega$, wave number $k^* = (\kappa^2 + \eta^2)^{1/2}$, zonal and meridional wave number components $\kappa$ and $\eta$, coefficient $\beta$ of meridional Coriolis parameter ($f$) change, $H$

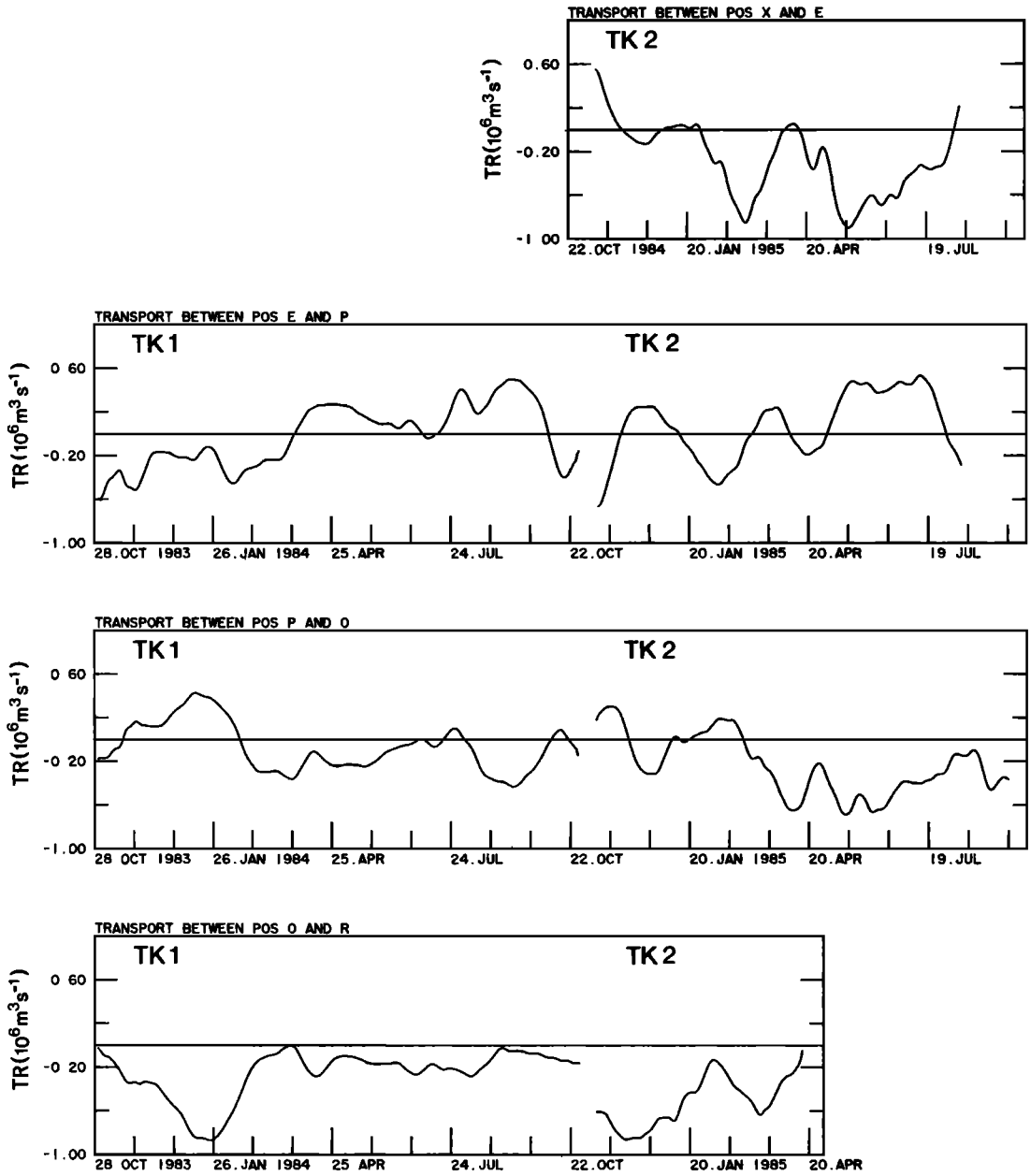


Fig. 12. Time series of relative transports (TR) across 28°N (see Figure 2 and Table 3) during two observational periods (TK1, TK2).

the vertical scale (water depth), $R$ the internal Rossby radius, and $N$ the Brunt-Väisälä frequency.

The latitudinal limit for baroclinic Rossby waves is given by

$$\omega \leq \omega_c = \frac{\beta NH}{2\pi f} \tag{3}$$

For $\beta = 2 \times 10^{-11}$ m$^{-1}$ s$^{-1}$, $f = 7.3 \times 10^{-5}$ s$^{-1}$, $\phi = 30°$ (latitude), $H = 5 \times 10^3$ m, and $N = 2 \times 10^{-3}$ s$^{-1}$, we obtain the period $\tau_c$ of the latitudinal limit:

$$\tau_c = \frac{2\pi}{\omega_c} \sim 160 \text{ days} \tag{4}$$

Therefore only baroclinic wave periods longer than 160 days are to be expected in our case. The dispersion relations for the two cases $\eta = 0$ and $|\kappa| = |\eta|$ are given in Figure 14, where dashed lines refer to annual and semiannual periods. The wavelength ranges in these two cases are indicated by the intervals in the lower part of the diagram. For annual waves we find possible wavelengths near 100 km and between 850 and 1250 km, for semiannual waves between 180 and 480 km. The distance between mooring R in the west and mooring X in the east is only about 830 km, and we will therefore study only the smaller spatial scales of expected annual and semiannual waves (100 and 180–480 km, respectively).

We first use a simple model assuming a linear superposi-

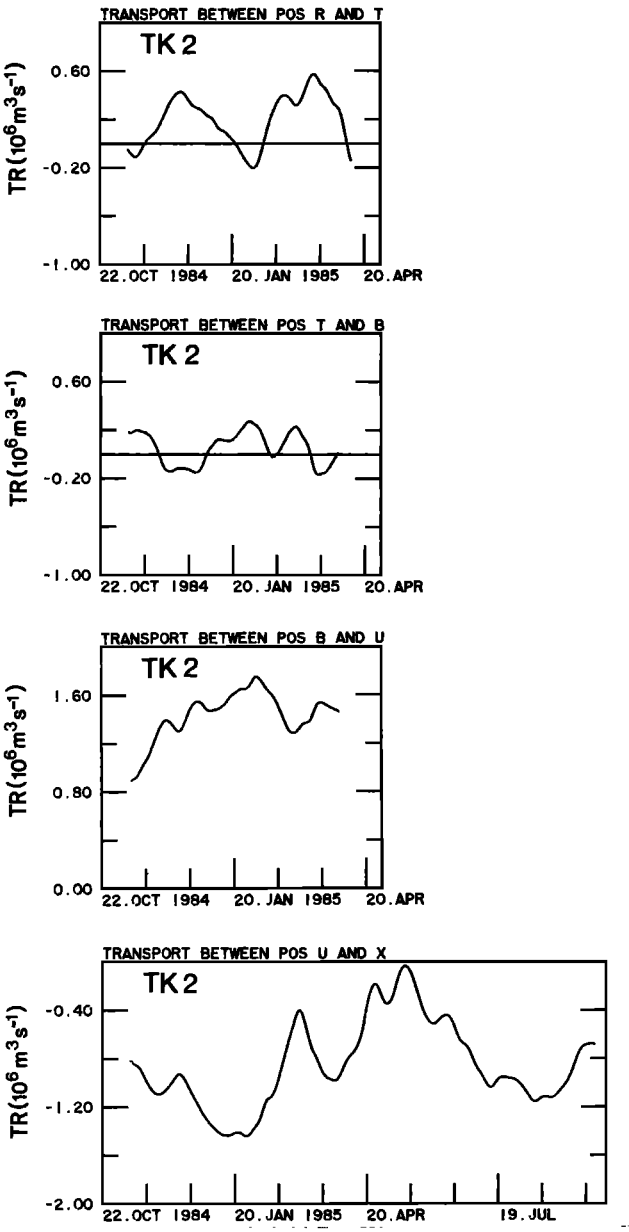


Fig. 13. Time series of relative transports (TR) across 27°W and across the line between moorings U and X (see Table 3) during second observational period (TK2).

tion of two propagating baroclinic waves of first order, without specifying Rossby wave dynamics, to describe the variability of meridional volume transports. The vertical structure function $F(z)$ is identical for both waves. For each time and position we can therefore, after subtraction of the temporal mean, separate the meridional velocity $v(x, z, t)$ into a vertically dependent ($F$) and a horizontally and time-dependent ($\bar{v}$) term:

$$v(x, z, t) = F(z)\bar{v}(x, t) \tag{5}$$

where $x$ is the eastward coordinate, $z$ the upward coordinate, and $t$ time.

Differentiation with respect to $z$ results in

$$\frac{\partial v(x, z, t)}{\partial z} = \frac{dF(z)}{dz}\bar{v}(x, t) \tag{6}$$

or

$$\bar{v}(x, t) = \left(\frac{dF(z)}{dz}\right)^{-1} \frac{\partial v(x, z, t)}{\partial z} \tag{7}$$

With $x_j$ ($j = 1, \cdots, 4$) half-way between the mooring positions along 28°N, time $t_k$ ($k = 1, \cdots, K$), and $z_A$ and $z_B$ equal to the depth range boundaries of the selected data set, we obtain

$$\bar{v}(x_j, t_k) \sim \frac{v(x_j, z_A, t_k) - v(x_j, z_B, t_k)}{F(z_A) - F(z_B)} \tag{8}$$

An inspection of CTD profiles leads to the conclusion that $v$ is sufficiently linear with depth in the range $z_A \le z \le z_B$. Therefore the equation can be used directly to determine $\bar{v}$. With $\bar{v}(x_j, t_k)$ known, the volume transport $M^D(x_j, t_k)$ through the area between adjacent stations with distance $\Delta x$ and between the surface and depth $z_0$ (with $z_0 = -1500$ m) can be calculated:

$$M^D(x_j,t_k) = \int_{x_j-(\Delta x/2)}^{x_j+(\Delta x/2)} \int_{z_0}^{0} F(z)\bar{v}(x_j,t_k)\, dz\, dx$$

$$= \int_{x_j-(\Delta x/2)}^{x_j+(\Delta x/2)} \bar{v}(x_j, t_k)\, dx \int_{z_0}^{0} F(z)\, dz \tag{9}$$

If the transport variations are caused by superimposed waves ($i$) at each time $t_K$, we obtain the wave model transport $M_I^W$ with $\bar{v}_i = A_i \sin(\kappa_i x - \omega_i t + \phi_i)$, where $\phi_i$ is phase:

$$M_I^W(x_j, t_k) = 2\int_{z_0}^{0} F(z)\, dz \left[\sum_{i=1}^{I} \frac{A_i}{\kappa_i} \sin(\kappa_i x_j - \omega_i t_k + \phi_i) \sin \kappa_i \Delta x\right] \tag{10}$$

Here we used the relation

TABLE 3. Selection of Data Sets for Simulation

| Data Version | Phase | End Point Moorings | | | | No. of Transport Series | Duration, days |
|---|---|---|---|---|---|---|---|
| | | O/R | P/O | E/P | X/E | | |
| D1 | TK1 | X | X | X | | 3 | 365 |
| D2 | TK2 | X | X | X | X | 4 | 157 |
| D3 | TK2 | | X | X | X | 3 | 277 |
| D4 | TK1/TK2 | X | X | X | | 3 | 432 |

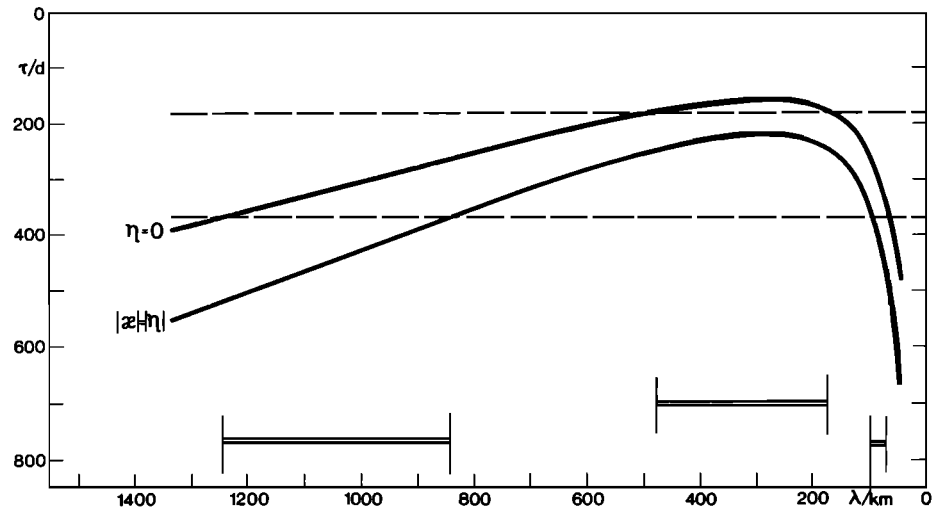


Fig. 14. Dispersion relation of first-order baroclinic Rossby waves for $\eta = 0$ and $\kappa = \eta$. The dashed lines indicate annual and semiannual periods ($\tau$), the double-line ranges give wavelength ($\lambda$) ranges for these periods.

TABLE 4. Wave Solutions for Transport Time Series From Model I (Baroclinic for Annual Periods (334–371 Days) and Semiannual Periods (182–210 Days), Barotropic for 90-Day Periods (87–92 Days))

| Data Version | No. | $\Delta F$, $\times 10^2$% | $A^*$, $10^1$ m$^2$ s$^{-1}$ | $\kappa$, $10^{-5}$ m$^{-1}$ | $\lvert\eta\rvert$, $10^{-5}$ m$^{-1}$ | $\lambda$, $10^3$ m | $T$, days | $\phi$, rad | $\lvert c\rvert$, $10^{-2}$ m s$^{-1}$ | $\lvert\alpha\rvert$, deg | $\lvert c_g\rvert$, $10^{-2}$ m s$^{-1}$ | $\lvert\delta\rvert$, deg |
|---|---|---|---|---|---|---|---|---|---|---|---|---|
| D1 | 1 | 0.18 | 2.1 | −1.83 | 0.78 | 316 | 183 | −1.7 | 2.0 | 23 | 0.9 | 42 |
| | | | 5.6 | −4.72 | 4.17 | 100 | 346 | −1.6 | 0.3 | 41 | 0.4 | 1 |
| | 2 | 0.18 | 2.1 | −1.83 | 0.78 | 316 | 183 | −0.7 | 2.0 | 23 | 0.9 | 42 |
| | | | 5.6 | −4.72 | 4.17 | 100 | 346 | 3.6 | 0.3 | 41 | 0.4 | 1 |
| | 3 | 0.18 | 1.9 | −1.58 | 0.44 | 383 | 183 | −0.6 | 2.4 | 16 | 1.0 | 65 |
| | | | 5.8 | −4.99 | 4.15 | 97 | 345 | −3.6 | 0.3 | 40 | 0.4 | 3 |
| | 4 | 0.18 | 2.0 | −1.83 | 0.74 | 318 | 182 | −0.6 | 2.0 | 22 | 0.9 | 42 |
| | | | 5.4 | −4.69 | 4.48 | 97 | 367 | −2.6 | 0.3 | 44 | 0.4 | 5 |
| | 5 | 0.18 | 1.8 | −1.59 | 0.46 | 379 | 183 | −3.4 | 2.4 | 16 | 1.0 | 63 |
| | | | 5.4 | −4.99 | 4.50 | 94 | 367 | −1.6 | 0.3 | 42 | 0.4 | 1 |
| D2 | 1 | 0.22 | 1.8 | −1.72 | 0.76 | 334 | 186 | −0.9 | 2.1 | 24 | 1.0 | 48 |
| | | | 4.5 | −1.57 | 1.21 | 317 | 91 | 1.4 | 4.0 | 38 | 5.1 | 15 |
| | 2 | 0.22 | 1.8 | −1.72 | 0.76 | 334 | 186 | 0.1 | 2.1 | 24 | 1.0 | 48 |
| | | | 4.5 | −1.57 | 1.21 | 317 | 91 | 1.4 | 4.0 | 38 | 5.1 | 15 |
| | 3 | 0.22 | 1.8 | −1.72 | 0.76 | 334 | 186 | 0.1 | 2.1 | 24 | 1.0 | 48 |
| | | | 4.5 | −1.56 | 1.19 | 320 | 90 | 1.4 | 4.1 | 37 | 5.2 | 15 |
| | 4 | 0.22 | 1.8 | −1.72 | 0.76 | 334 | 186 | 0.1 | 2.1 | 24 | 1.0 | 48 |
| | | | 4.5 | −1.57 | 1.21 | 317 | 91 | 1.4 | 4.0 | 38 | 5.1 | 15 |
| | 5 | 0.21 | 1.6 | −1.64 | 1.23 | 306 | 210 | 0.1 | 1.7 | 37 | 1.3 | 45 |
| | | | 3.9 | −1.57 | 1.19 | 319 | 90 | 0.4 | 4.1 | 37 | 5.1 | 16 |
| D3 | 1 | 0.20 | 2.7 | −1.63 | 2.95 | 186 | 371 | −0.9 | 0.6 | 61 | 1.1 | 50 |
| | | | 2.7 | −1.90 | 0.97 | 295 | 87 | 0.6 | 3.9 | 27 | 4.4 | 36 |
| | 2 | 0.27 | 2.5 | −1.90 | 0.97 | 295 | 87 | 3.6 | 3.9 | 27 | 4.4 | 36 |
| | | | 719 | — | — | 200 | ∞ | −1.6 | — | — | — | — |
| | 3 | 0.23 | 2.7 | −1.64 | 2.76 | 196 | 345 | −0.1 | 0.7 | 59 | 1.1 | 48 |
| | | | 4.3 | −4.25 | — | — | 148 | 0.2 | — | — | — | — |
| | 4 | 0.27 | 2.6 | −1.79 | 0.92 | 312 | 189 | 3.4 | 1.94 | 27 | 1.0 | 41 |
| | | | 812 | −3.14 | — | 200 | ∞ | −1.6 | — | — | — | — |
| | 5 | 0.23 | 2.8 | −2.06 | 0.98 | 275 | 92 | 0.1 | 3.5 | 26 | 3.8 | 39 |
| | | | 1.7 | −1.64 | 0.82 | 343 | 191 | 0.6 | 2.1 | 26 | 1.1 | 50 |
| D4 | 1 | 0.27 | 1.6 | −1.49 | 2.49 | 216 | 334 | −0.6 | 0.8 | 59 | 1.3 | 51 |
| | | | 1.0 | −4.19 | 4.13 | 107 | 346 | 2.1 | 0.4 | 45 | 0.4 | 8 |
| | 2 | 0.25 | 1.6 | −1.71 | — | — | 173 | 0.5 | — | — | — | — |
| | | | 2.3 | −2.39 | — | — | 85 | −1.4 | — | — | — | — |
| | 3 | 0.28 | 2.0 | −1.78 | — | — | 171 | 1.9 | — | — | — | — |
| | | | 1.7 | −1.79 | 0.32 | 346 | 174 | 0.5 | 2.3 | 2 | 0.7 | 62 |
| | 4 | 0.26 | 1.6 | −1.72 | — | — | 173 | 0.5 | — | — | — | — |
| | | | 2.3 | −2.40 | — | — | 85 | 1.4 | — | — | — | — |
| | 5 | 0.27 | 1.6 | −1.72 | — | — | 170 | 0.6 | — | — | — | — |
| | | | 2.1 | −2.39 | — | — | 85 | 1.4 | — | — | — | — |

$\Delta F$ is the mean deviation of the data from the simulation in percent. Free parameters for fitting: $A^*$, amplitude; $\kappa$, zonal wave number; $T$, period; and $\phi$, phase. Computed parameters in the case of Rossby wave dynamics: $\eta$, meridional wave number; $\lambda$, wavelength; $c$, phase velocity; $\alpha$, angle between phase velocity and westward coordinate; $c_g$, group velocity; and $\delta$, angle between group velocity and north-south line.

TABLE 5. Baroclinic Wave Solutions for Transport Time Series From Model II

| Data Version | No. | $\Delta F$, $\times 10^2$% | $A^*$, $10^1$ m$^2$ s$^{-1}$ | $\kappa$, $10^{-5}$ m$^{-1}$ | $\lambda_x$, $10^3$ m | $T$, days | $\phi$, rad | $c_x$, $10^{-2}$ m s$^{-1}$ | $c_{gx}$, $10^{-2}$ m s$^{-1}$ |
|---|---|---|---|---|---|---|---|---|---|
| D1 | 1 | 0.23 | 2.5 | −1.50 | 419 | 173 | −0.2 | −2.8 | −1.1 |
| | | | 4.0 | −4.33 | 145 | 199 | −2.3 | −0.8 | 0.5 |
| | 2 | 0.24 | 1.9 | −1.63 | 385 | 168 | −0.3 | −2.7 | −0.8 |
| | | | 3.0 | −2.89 | 217 | 167 | 2.5 | −1.5 | 0.3 |
| | 3 | 0.24 | 1.9 | −1.67 | 376 | 167 | −0.3 | −2.6 | −0.8 |
| | | | 290 | −3.14 | 200 | 172 | 2.2 | −1.3 | 0.4 |
| | 4 | 0.23 | 2.4 | −1.46 | 430 | 175 | −0.2 | −2.8 | −1.1 |
| | | | 4.1 | −4.27 | 147 | 198 | −2.2 | −0.9 | 0.5 |
| | 5 | 0.23 | 2.5 | −1.50 | 419 | 173 | −0.2 | −2.8 | −1.1 |
| | | | 4.0 | −4.33 | 145 | 200 | −2.3 | −0.8 | 0.5 |
| D1 | 1 | 0.32 | 45.4 | −2.04 | 308 | 161 | −0.2 | −2.2 | −0.2 |
| | | | 46.4 | −2.06 | 305 | 162 | −0.7 | −2.2 | −0.2 |
| | 2 | 0.30 | 9.0 | −1.08 | 582 | 203 | −0.3 | −3.3 | −2.0 |
| | | | 36.4 | −4.14 | 152 | 195 | −0.1 | −0.9 | 0.5 |
| | 3 | 0.32 | 45.8 | −2.04 | 308 | 161 | −0.2 | −2.2 | −0.2 |
| | | | 46.7 | −2.06 | 305 | 162 | 0.7 | −2.2 | −0.2 |
| | 4 | 0.30 | 9.0 | −1.08 | 582 | 203 | −0.8 | −3.3 | −2.0 |
| | | | 36.5 | −4.14 | 152 | 195 | −0.1 | −0.9 | 0.5 |
| | 5 | 0.30 | 6.1 | −1.09 | 576 | 203 | −0.3 | −3.3 | −2.0 |
| | | | 25.2 | −4.11 | 153 | 194 | −0.1 | −0.9 | 0.5 |
| D3 | 1 | 0.23 | 1.4 | −1.37 | 459 | 179 | −0.3 | −3.0 | −1.3 |
| | | | 14.8 | −7.85 | 80 | 311 | 0.2 | −0.3 | 0.3 |
| | 2 | 0.30 | 0.8 | −1.04 | 604 | 207 | 0.4 | −3.4 | −2.1 |
| | | | 0.5 | −4.19 | 150 | 196 | −0.1 | −0.9 | 0.5 |
| | 3 | 0.30 | 0.9 | −1.24 | 507 | 189 | −0.5 | −3.1 | −1.6 |
| | | | 556 | −3.14 | 200 | 172 | 0.1 | −1.3 | 0.4 |
| | 4 | 0.32 | 1.0 | −1.07 | 587 | 204 | 0.3 | −3.3 | −2.0 |
| | | | 0.8 | −2.78 | 226 | 166 | 0.2 | −1.6 | 0.3 |
| | 5 | 0.30 | 1.3 | −1.05 | 598 | 206 | 0.3 | −3.4 | −2.1 |
| | | | 0.4 | −3.89 | 162 | 188 | −0.2 | −1.0 | 0.5 |
| D4 | 1 | 0.28 | 1.2 | −1.47 | 427 | 174 | 0.0 | −2.8 | −1.1 |
| | | | 1.4 | −1.86 | 338 | 163 | 0.3 | −2.4 | −0.5 |
| | 2 | 0.28 | 1.2 | −1.47 | 427 | 174 | 0.0 | −2.8 | −1.1 |
| | | | 1.4 | −1.86 | 338 | 163 | 0.3 | −2.4 | −0.5 |
| | 3 | 0.29 | 1.2 | −1.51 | 416 | 173 | 0.0 | −2.8 | −1.0 |
| | | | 1.6 | −1.83 | 343 | 164 | 0.3 | −2.4 | −0.5 |
| | 4 | 0.28 | 0.9 | −1.45 | 433 | 175 | 0.1 | −2.9 | −1.2 |
| | | | 1.7 | −1.77 | 355 | 165 | 0.3 | −2.5 | −0.6 |
| | 5 | 0.28 | 0.9 | −1.45 | 433 | 175 | −0.1 | −2.9 | −1.2 |
| | | | 1.7 | −1.77 | 355 | 165 | 0.3 | −2.5 | −0.6 |

$\Delta F$ is the mean deviation of the data from the simulation in percent. Free parameters for fitting: $A^*$, $\kappa$, and $\phi$. Computed parameters: $\lambda_x$, zonal wavelength; $T$, period; $c_x$, zonal phase velocity component; and $c_{gx}$, zonal group velocity component (for further explanations, see Table 4).

TABLE 6. Typical Wave Properties Obtained From Model I (Baroclinic for Annual and Semiannual Periods, Barotropic for 90-Day Period)

| | Annual Period, 100-km Wavelength | Annual Period, 200-km Wavelength | Semiannual Period | 90-Day Period |
|---|---|---|---|---|
| $\lambda$, $10^3$ m | 98 ± 4 | 199 ± 15 | 335 ± 23 | 306 ± 16 |
| $T$, days | 352 ± 10 | 350 ± 19 | 186 ± 8 | 89 ± 1 |
| $A^*$, $10^1$ m$^2$ s$^{-1}$ | 4.8 ± 1.9 | 2.3 ± 0.6 | 1.9 ± 0.3 | 3.7 ± 0.9 |
| $\Delta$TR, $10^6$ m$^3$ s$^{-1}$ | 2.0 ± 0.8 | 2.3 ± 1.0 | 2.2 ± 0.3 | 3.6 ± 1.7 |
| $U_{max}$, $10^{-2}$ m s$^{-1}$ | 6.3 ± 2.4 | 3.0 ± 0.8 | 2.5 ± 0.3 | 4.9 ± 1.2 |
| $\lvert c \rvert$, $10^{-2}$ m s$^{-1}$ | 0.33 ± 0.02 | 0.66 ± 0.08 | 2.09 ± 0.2 | 3.95 ± 0.21 |
| $\lvert \alpha \rvert$, deg | 42 ± 1 | 59 ± 1 | 22 ± 6 | 33 ± 5 |
| $\lvert c_g \rvert$, $10^{-2}$ m s$^{-1}$ | 0.39 ± 0.03 | 1.16 ± 0.1 | 0.99 ± 0.14 | 4.78 ± 0.5 |
| $\lvert \delta \rvert$, deg | 1 ± 3 | 49 ± 1 | 49 ± 8 | 23 ± 11 |

Here, $\lambda$, wavelength; $T$, period; $A^*$, amplitude; $\Delta$TR, transport change amplitude; $U_{max}$, particle speed; $c$, phase velocity; $\alpha$, propagation direction relative to westward; $c_g$, group velocity; $\delta$, group velocity direction relative to southward. Error estimates result from averaging model results.

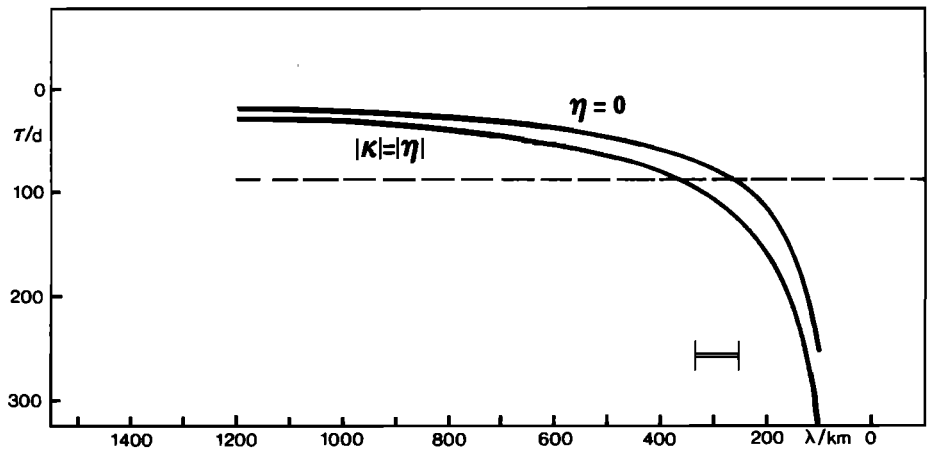


Fig. 15. Dispersion relation of barotropic Rossby waves for $\eta = 0$ and $\kappa = \eta$. The dashed line indicates the 90-day period ($\tau$), and the double-line range gives the wavelength ($\lambda$) range for this period.

$$\cos \gamma_1 - \cos \gamma_2 = -2 \sin \frac{\gamma_1 + \gamma_2}{2} \sin \frac{\gamma_1 - \gamma_2}{2} \qquad (11)$$

with

$$\gamma_1 = \kappa_i \left( x_j + \frac{\Delta x}{2} \right) - \omega_i t + \phi_i$$

$$\gamma_2 = \kappa_i \left( x_j - \frac{\Delta x}{2} \right) - \omega_i t + \phi_i$$

Assuming two wave components ($I = 2$), the relative transport is determined by least squares fitting of the observed $M$:

$$\sum_{j=1}^{J} \sum_{k=1}^{K} |M^D(x_j, t_k) - M_2^W(x_j, t_k)|^2 = \min \qquad (12)$$

$$F(\mathbf{X}) = \sum_{n=1}^{\tilde{N}} |f_n(\mathbf{X})|^2 = \min \qquad (13)$$

with $\tilde{N} = JK$ and $\mathbf{X} = (X_1, X_2, \cdots, X_Q)^T$ and $\tilde{N} > Q$.

$\mathbf{X}$ is the vector representing the variables $A_i$, $\kappa_i$, $\omega_i$, and $\phi_i$ of the elementary waves. Starting with a first guess, a Gauss-Newton algorithm [*Gill and Murray*, 1978] is used to determine the minimum value $\mathbf{X}^*$. The deviation between the data and the simulation is then given by $S$:

$$S = \left( \frac{1}{\tilde{N}} \sum_{n=1}^{\tilde{N}} |f_n(\mathbf{X}^*)|^2 \right)^{1/2} \qquad (14)$$

Up to this point we have not applied any restrictions required in the case of Rossby waves, but have only assumed the existence of two superimposed propagating waves with a vertical structure corresponding to a first mode. We call this our model I:

$$\mathbf{X} = (A_1, A_2, \kappa_1, \kappa_2, \omega_1, \omega_2, \phi_1, \phi_2)^T \qquad (15)$$

In a comparison with the Rossby wave dispersion relation, we can check whether the results are consistent with Rossby wave dynamics and, if so, what meridional wave numbers result in that case.

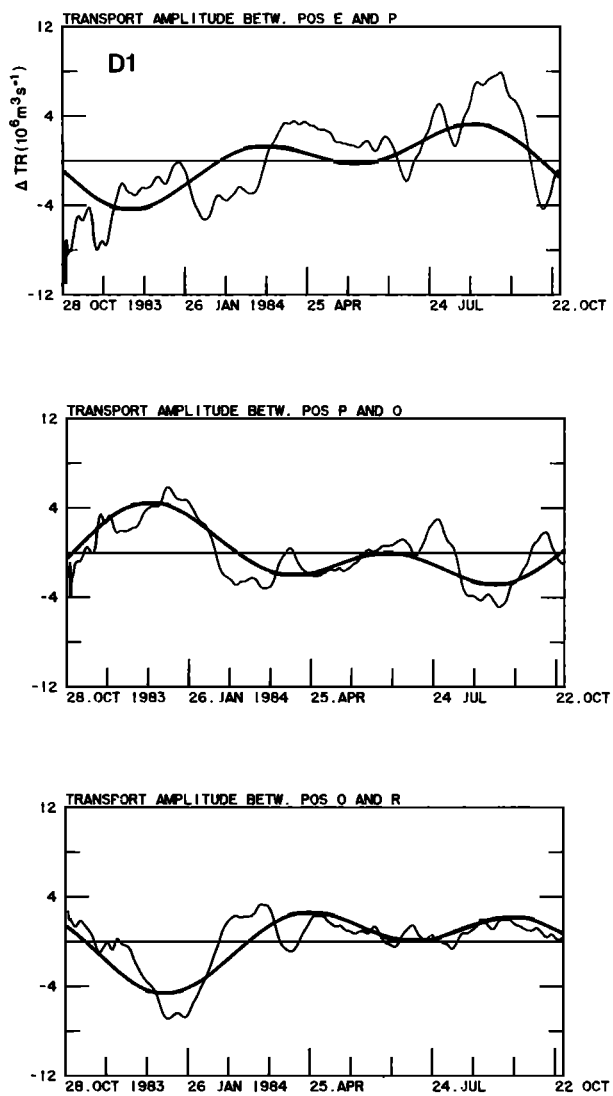


Fig. 16. Examples of amplitudes ($\Delta$TR) of measured relative transport time series and simulations by two superimposed propagating first-order baroclinic waves in model I for series D1 with 1-year duration and three station pairs.

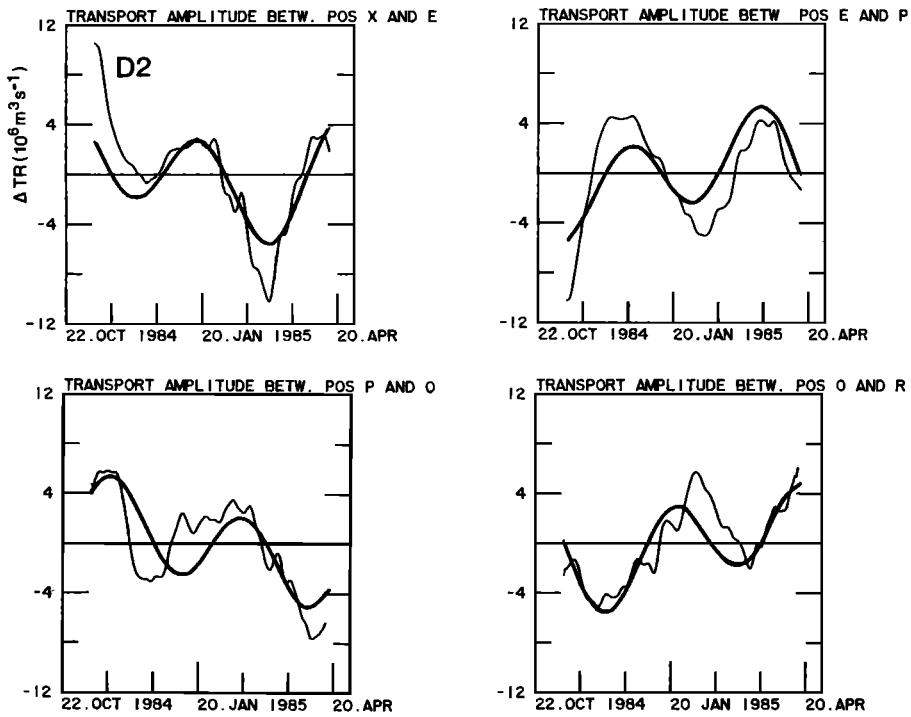


Fig. 17. Examples of amplitudes (ΔTR) of measured relative transport time series and simulations by two superimposed propagating first-order baroclinic waves in model I for series D2 with half-year duration and four station pairs.

In a second model we assume westward propagating Rossby waves with $\eta = 0$, and we use the particular Rossby wave dispersion relation:

$$\mathbf{X} = (A_1, A_2, \kappa_1, \kappa_2, \phi_1, \phi_2)^T \qquad (16)$$

with

$$\omega_i = -\frac{\beta \kappa_i}{\kappa_i^2 + R^{-2}} \qquad i = 1, 2$$

This will be our model II.

## 6. Model Results

Various combinations of the data sets were used for the simulation. They had different spatial and temporal coverage and are summarized in Table 3. The ranges of wavelengths and periods which could be determined directly from the data are $2\Delta x \le \lambda \le L$ and $2\Delta t \le \tau \le D$, where $\Delta x$ is the mooring separation as defined before, $\Delta t$ is given by $t_{k+1} - t_k$, $L$ is the maximum separation of $x_j$, and the maximum duration of the version considered is given by $D$.

The spatial sampling distances are too large to cover all wave numbers given in the ranges of Figure 14 independently. The temporal sampling, however, is adequate for periods of a few months to a year. By coupling the spatial and temporal information through the propagating wave model, we can use the temporal variations at the given positions to arrive at period and wavelength estimates.

The first guesses needed for the start of the estimates were obtained from the visual inspection of the transport time series. Apparent periods and wavelengths were identified, and different initial guesses were obtained by increasing and decreasing these values within reasonable ranges. The numbers 1–5 in Tables 4 and 5 refer to such different initial guesses. Linear trends were removed. The solutions ob-

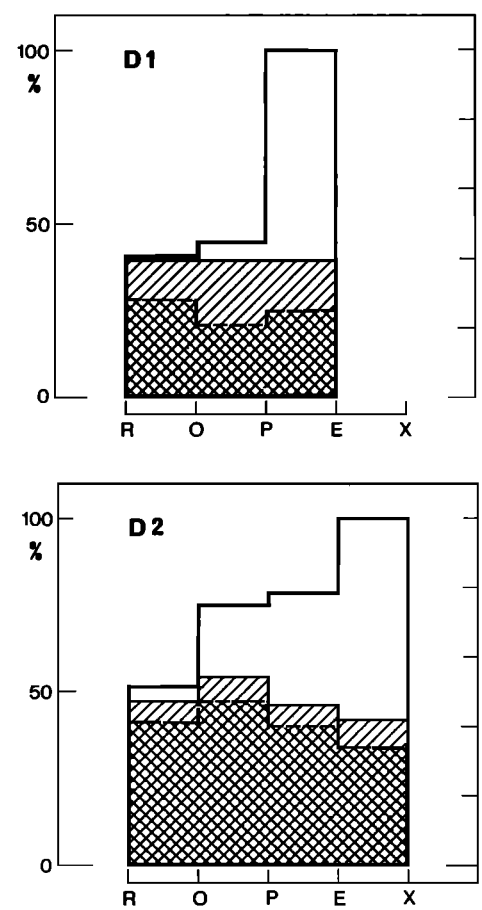


Fig. 18. Variance of relative transport observations (open area, easternmost value set to 100%) and variance of two approximations (hatched and crossed area) with model I for a one-year (D1) and half-year (D2) duration.

tained for model I are presented in Table 4, those for model II in Table 5. $\Delta F$ is $S$ normalized by the maximum transport value $M^D$ of the version considered. Small values of $\Delta F$ indicate a good simulation. The amplitude is given by

$$A^* = A \int_{z_0}^{0} F(z)\, dz$$

The results indicate a lower mean deviation of the data from the simulation for model I than for model II. All the results in Table 4 not consistent with baroclinic Rossby wave dynamics are found at the short periods of approximately 90 days primarily resulting from versions D2 and D3. Because of the shortness of these versions, the short-period variations play a more prominent role in approximating the observed changes. Two cases with extreme $A^*$ (period $\rightarrow\infty$) are affected by numerical instability. In all data versions of model I, we find wavelengths between 300 and 360 km with semiannual periods. Major differences are found for the second wave. In the cases of the long data series in version D1 we find mostly annual waves with short wavelengths of about 100 km. For versions D3 and D4 we also find annual waves with longer wavelengths, about 200 km.

Combining the values of free parameters in Table 4 with the baroclinic Rossby wave dispersion relation, a meridional wave number (except for its sign) and also phase and group velocities can be determined for annual and semiannual signals. We can obtain information on the sign of the dominant meridional wave number from the Reynolds stress term $u'v'$. *Müller and Siedler* [1992] obtained significant numbers for moorings R and O (see their Table A3). The value is positive, indicating a phase propagation to the southwest.

The main results are summarized in Table 6. In order to check whether changes in the choice of $N$ and $H$ could be important, these values were varied in ranges probable in the area. Typical variations in period $T$ caused by these changes are of similar magnitude as the uncertainty of the simulation given in Table 6.

In addition to cases with annual and semiannual periods, signals of 90-day period were found. They can be interpreted as an effect of a barotropic Rossby wave. In a horizontally homogeneous ocean, such waves would not generate temperature variability at a fixed position. If horizontal temperature gradients exist, however, barotropic waves will produce temperature changes. With the limited depth range of our thermistor cables, such changes will show up both when fitting the data to a vertically constant mode or to a first-order baroclinic mode with approximately constant vertical gradient in the given depth range. We did not consider it useful to actually fit to a barotropic mode, since the variability is related to unknown horizontal temperature gradients. If such a signal occurs, however, in the baroclinic mode analysis, its period and wavelength can be related to the generating barotropic wave. The dispersion relationships for barotropic Rossby waves with $\eta = 0$ and $|\kappa| = |\eta|$ are presented in Figure 15. The observed 90-day wave signal corresponds to a barotropic wave propagating to approximately $\pm 25°$ off the westward direction.

The model II simulations presented in Table 5 are of lower quality (larger $\Delta F$). Wavelengths are between 150 and 600 km. It is reassuring, however, that with pure westward propagation required, almost all periods are about half-year where model I indicates the smallest deviations from westward propagation.

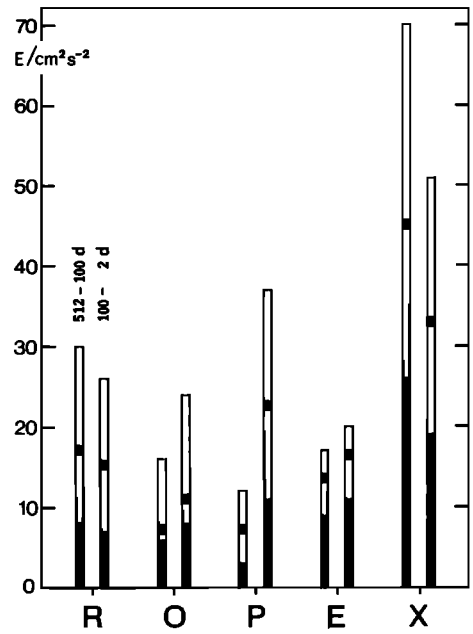


Fig. 19. Spectral estimates of energy ($E$) for the two period ranges indicated, obtained from the current meters at moorings R, O, P, E, X (see Figures 2 and 5). The short solid line gives the value, and the open area indicates the 95% confidence limits.

Examples of observed and simulated time series in model I are shown in Figures 16 and 17. In Figure 18 we display the transport variance between moorings for two simulations, normalized with the maximum variance in each series. Obviously, the simulation is much better in the western part of the array than in the east. In the area with poor approximation, we earlier found an unusual behavior in the transport variability obtained from quasi-synoptic CTD casts (Figure 9), with predominant northward transports opposite to the gyre flow direction. In this eastern region the low-frequency currents are much more energetic than further west. This is also documented in Figure 19 by the spectral estimates obtained from the current meters in the moored array. The higher values close to the Canary archipelago are found both at the annual to semiannual wave periods (512–100 days) and at shorter time scales (100–2 days).

## 7. Discussion

Our analysis leads to the conclusion that superpositions of two first-order baroclinic waves with annual and with semiannual periods and a barotropic wave with a 90-day period provide good approximations of low-frequency variability at some distance to the west of the Canary archipelago. This is consistent with Rossby wave dynamics, although other processes may also play a role. The approximation, however, is poor within 200 km of the islands.

Most earlier studies have concentrated on annual Rossby waves with longer wavelengths of order 1000 km. Our results indicate annual contributions at shorter wavelengths of 100–200 km and semiannual components at 300 km which are consistent with baroclinic Rossby wave dynamics. Earlier observations in the eastern subtropical North Pacific [*Kang and Magaard*, 1980] and wind-driven Rossby wave models for the eastern North Atlantic [*Hermann and Krauss*, 1989] arrived at a northwestward direction of propagation. When assuming

Rossby wave dynamics, the Reynolds stress in our data indicates a southwestward propagation of the dominating wave. In the case of baroclinic waves with annual periods and 100- to 200-km wavelength, this leads to about 45°–60° deviation to the south from westward propagation, and in the case of the semiannual waves to a direction closer to westward, with a deviation of about 25°. The direction of the barotropic waves is ±25° off the westward direction.

The large differences between observation and simulation in the eastern part of the studied region can be due to the particular flow patterns close to the Canary archipelago or occur because of the existence of a source region for the generation of the waves which are observed further west. The first possibility cannot be discounted because the eastern part of the observational area was situated close to the Canary Islands, with the Canary Current passing the archipelago from north to south. Topographically controlled quasi-permanent eddies can be expected to exist, changing slowly in structure and intensity and causing low-frequency current variability. Information on the particular properties of flow near the archipelago is too scarce, however, to provide any firm evidence for such a process.

We cannot identify the generation process for the wave contributions in the area from our data. Various mechanisms have been proposed in earlier studies: wind stress forcing locally [*White and Saur*, 1981] or on larger scales [*Magaard*, 1977; *Price and Magaard*, 1980, 1983; *Krauss and Wübber*, 1982; *Lippert and Käse*, 1985; *Hermann and Krauss*, 1989], buoyancy forcing [*Magaard*, 1977], atmospheric pressure forcing [*Magaard*, 1977], forcing by an annual change of nearby along-shore currents [*Mysak*, 1983], and forcing by coastal Kelvin waves which have been wind forced in the equatorial belt and propagate poleward along the eastern boundary [*Pares-Sierra and O'Brien*, 1989; *Johnson and O'Brien*, 1990].

As was shown by *Magaard* [1977], atmospheric pressure changes and buoyancy changes are negligible. Local or remote wind stress forcing are possible mechanisms. But with the strong change in current magnitude and direction west of the Canary Islands, the process proposed by *Mysak* [1983] is also conceivable.

*Acknowledgments.* We thank the staff of the Marine Physics department at the Institut für Meereskunde of Kiel University for assistance in observations and data processing. We appreciate the help of the captains and crews of the research vessels *Meteor*, *Poseidon*, and *Polarstern* during the observational programs. We have benefited from discussions with T. J. Müller, M. Schröder, and K. Speer during the analysis and from the comments of an unknown reviewer on the barotropic wave contributions. The study was funded by the Deutsche Forschungsgemeinschaft (SFB 133).

## REFERENCES

Emery, W. J., and J. S. Dewar, Mean temperature-salinity, salinity-depth, and temperature-depth curves from the North Atlantic and the North Pacific, *Prog. Oceanogr.*, *11*, 219–305, 1982.

Emery, W. J., and L. Magaard, Baroclinic Rossby waves as inferred from temperature fluctuations in the eastern Pacific, *J. Mar. Res.*, *34*, 365–385, 1976.

Gill, P. E., and W. Murray, Algorithms for the solution of nonlinear least squares problem, *SIAM J. Numer. Anal.*, *15*, 977–992, 1978.

Gould, W. J., Physical oceanography of the Azores Front, *Prog. Oceanogr.*, *14*, 167–190, 1985.

Hermann, P., and W. Krauss, Generation and propagation of annual Rossby waves in the North Atlantic, *J. Phys. Oceanogr.*, *19*, 727–744, 1989.

Johnson, M. A., and J. J. O'Brien, The northeast Pacific Ocean response to the 1982–1983 El Niño, *J. Geophys. Res.*, *95*, 7155–7166, 1990.

Kang, Y. Q., and L. Magaard, Stable and unstable Rossby waves in the North Pacific current as inferred from the mean stratification, *Dyn. Atmos. Oceans*, *3*, 1–14, 1979.

Kang, Y. Q., and L. Magaard, Annual baroclinic Rossby waves in the central North Pacific, *Phys. Oceanogr.*, *10*, 1159–1167, 1980.

Käse, R. H., and G. Siedler, Meandering of the subtropical front southeast of the Azores, *Nature*, *300*(5889), 245–246, 1982.

Käse, R. H., W. Zenk, T. B. Sanford, and W. Hiller, Currents, fronts, and eddy fluxes in the Canary Basin, *Prog. Oceanogr.*, *14*, 231–257, 1985.

Klein, B., and G. Siedler, On the origin of the Azores Current, *J. Geophys. Res.*, *94*, 6159–6168, 1989.

Krauss, W., and C. Wübber, Response of the North Atlantic to annual wind variations along the eastern coast, *Deep Sea Res.*, *29*, 851–868, 1982.

LeBlond, P. H., and L. A. Mysak, *Waves in the Ocean*, 602 pp., Elsevier, New York, 1978.

Lippert, A., and R. H. Käse, Stochastic wind forcing of baroclinic Rossby waves in the presence of a meridional boundary, *J. Phys. Oceanogr.*, *15*, 184–194, 1985.

Magaard, L., On the generation of baroclinic Rossby waves in the ocean by meteorological forces, *J. Phys. Oceanogr.*, *7*, 359–364, 1977.

Magaard, L., On the potential energy of baroclinic Rossby waves in the North Pacific, *J. Phys. Oceanogr.*, *13*, 38–42, 1983.

Magaard, L., and J. M. Price, Note on the significance of a previous Rossby wave fit to internal temperature fluctuations in the eastern Pacific, *J. Mar. Res.*, *35*, 649–651, 1977.

McWilliams, J. C., and G. R. Flierl, Optimal, quasi-geostrophic wave analyses of MODE array data, *Deep Sea Res.*, *23*, 285–300, 1976.

McWilliams, J. C., and A. Robinson, A wave analysis of the Polygon array in the tropical Atlantic, *Deep Sea Res.*, *21*, 359–368, 1974.

MODE Group, The Mid-Ocean Dynamics Experiment, *Deep Sea Res.*, *25*, 859–910, 1978.

Müller, T. J., and G. Siedler, Multiyear current time series in the eastern North Atlantic Ocean, *J. Mar. Res.*, *50*, 1–37, 1992.

Mysak, L., Generation of annual Rossby waves in the North Pacific, *J. Phys. Oceanogr.*, *13*, 1908–1923, 1983.

Pares-Sierra, A., and J. J. O'Brien, The seasonal and interannual variability of the California Current system: A numerical model, *J. Geophys. Res.*, *94*, 3159–3180, 1989.

Price, J. M., and L. Magaard, Rossby wave analysis of the baroclinic potential energy in the upper 500 meters of the North Pacific, *J. Mar. Res.*, *38*, 249–264, 1980.

Price, J. M., and L. Magaard, Rossby wave analysis of subsurface temperature fluctuations along the Honolulu–San Francisco Great Circle, *J. Phys. Oceanogr.*, *13*, 258–268, 1983.

Schmitz, W. J., Jr., J. F. Price, and P. L. Richardson, Recent moored current meter and SOFAR float observations in the eastern Atlantic near 32N, *J. Mar. Res.*, *46*, 301–319, 1988.

Siedler, G., and L. Stramma, The applicability of the *T*/*S* method to geopotential anomaly computations in the northeast Atlantic, *Oceanol. Acta*, *6*(2), 167–172, 1983.

Stramma, L., Geostrophic transport in the warm water sphere of the eastern subtropical North Atlantic, *J. Mar. Res.*, *42*, 537–558, 1984.

White, W. B., Annual forcing of baroclinic long waves in the tropical North Pacific, *J. Phys. Oceanogr.*, *7*, 50–61, 1977.

White, W. B., Traveling wavelike mesoscale perturbations in the North Pacific current, *J. Phys. Oceanogr.*, *12*, 231–243, 1982.

White, W. B., and J. F. T. Saur, A source of annual baroclinic waves in the eastern subtropical North Pacific, *J. Phys. Oceanogr.*, *11*, 1452–1462, 1981.

M. Finke and G. Siedler, Institut für Meereskunde, Dusternbrooker Weg 20, W-2300 Kiel, Germany.

(Received April 22, 1991;
revised August 12, 1992;
accepted August 13, 1992.)